communications materials

Article

https://doi.org/10.1038/s43246-024-00560-x

Correlated electron physics near a site-selective pressure-induced Mott transition in α-$LiFe_5O_8$

Samar Layek [1,2,3] ✉, **Eran Greenberg** [2,4,6], **Davide Levy** [2], **Vitali Prakapenka** [4], **Siddharth S. Saxena** [1,5] ✉ & **Gregory Kh. Rozenberg** [2] ✉

The Mott insulator-to-metal transition (IMT) driven by electron correlations has been among the main research topics in materials science over the past decades. The complex interplay between electronic and lattice degrees of freedom leads to various transition scenarios. Of particular interest may be the case of a transition involving the formation of complex phases comprising regions that differ significantly in their physical properties within the same material. Here, we present the results that advance the understanding of the IMT phenomenon, offering the documentation of a pure site-selective mechanism that is not complicated by any structural and spin transformation. Combining XRD, resistivity, Mössbauer and Raman spectroscopy measurements, we provide evidence for a pure pressure-induced Mott transition in α-$LiFe_5O_8$, characterized by site-selective delocalization of electrons, leading to the formation, above ~65 GPa, of a site-selective Mott phase consisting of metallic and insulating sublattices. We note that the electron delocalization in the partially disordered octahedral sublattice cannot be understood purely in terms of a Mott transition, the Anderson-Mott transition picture seems more adequate.

The insulator-metal transition (IMT) driven by electronic correlations is one of the most fundamental concepts in condensed matter. The complex interplay between electronic correlations and the spin, orbital, and lattice degrees of freedom leads to a wealth of possible scenarios of the IMT and the appearance of complex phases, which could be attractive for technological applications. The connective Mott transition, is of particular importance because it is essential to understanding the properties of strongly correlated transition-metal compounds being especially relevant to understanding high-temperature superconductivity, as well as heavy-fermion behavior[1–8]. A definitive electronic phenomenon in such compounds, induced by pressure, composition, or other means, is the breakdown of the *d*- or *f*-electron localization, causing the Mott IMT, which usually goes along with a collapse of the magnetic interactions[1–3,9,10] or a high- to low-spin (HS-LS) transition[11–14].

Of particular interest is the case of the Mott IMT in materials with a crystal structure containing transition-metal cations in different coordination polyhedra, where the interplay of electronic correlations and crystal structure may result in rather complex behavior of the electronic and magnetic states. Recent theoretical calculations of rare-earth nickelates[15,16] suggest the formation of a Mott phase that remains electrically insulating while exhibiting the formation of site-selective local moments and Ni–*d*, O–*p* singlet states. Furthermore, high-pressure (HP) studies of Fe_2O_3 suggest that this material undergoes a site-selective Mott transition, accompanied by a site-dependent collapse of magnetic moments[17] (which goes along with site-dependent delocalization (metallization) of the 3*d* electrons). However, in Fe_2O_3 the electron delocalization corroborating with the spin transition coincides also with a structural phase transition, all these complicating an analysis of the role of structural and electronic components in the transition. Undoubtedly, additional studies of the phenomenon of the site-selective Mott transition are essential to further understanding of its features.

Ferrite oxides and particularly ferric spinels seem to be suitable objects for the study of the site-selective Mott IMT phenomenon since their structures are usually characterized by two distinct coordination sites suggesting that in these systems a delocalization/metallization of the 3*d* electrons should not occur simultaneously and propagate through different crystallographic sites at different degrees of compression[17,18]. We note that ferrite spinels are some of the most studied materials, not only due to their

---

[1]Cavendish Laboratory, JJ Thomson Avenue, University of Cambridge, Cambridge, CB3 0HE, UK. [2]School of Physics and Astronomy, Tel-Aviv University, Tel-Aviv, Israel. [3]Department of Physics, Applied Science Cluster, UPES, Dehradun, Uttarakhand, India. [4]Center for Advanced Radiation Sources, University of Chicago, Chicago, Illinois, USA. [5]British Management University Tashkent, 35 Bobur Mirza Street, Tashkent, Uzbekistan. [6]Present address: Applied Physics Division, SNRC, Yavne, Israel. ✉e-mail: samarlayek@gmail.com; sss21@cam.ac.uk; emtsm@tauex.tau.ac.il

rich physical properties, but also diverse applications in the field of magnetic recording media, ferrofluid, gas sensing, soft or hard magnetic materials, microwave absorption, etc.[19–21]. Most of the above-mentioned materials order magnetically above room temperature demonstrating a variety of magnetic ordering types, and their properties can be altered by doping[20,21], or application of pressure[22,23].

In the particular case of ferric oxides, the Mott and spin transitions are usually first-order transitions observed at the 40–60 GPa pressure range[10,13,24,25]. However, a signature of a partial sluggish second-order HS-LS transition has been found recently for some ferrite post-spinels[26] and in disordered α-LiFeO$_2$, characterized by a random distribution of Li and Fe ions[27]. Sluggish partial site-specific spin crossover appears to be the preferred electronic response of ferrous spinels at sufficiently high density[28–30]. Noteworthy, at high pressures, all these materials are characterized by the random environment of Fe ions, and specific features of the Mott IMT in case of such disordered systems are of particular interest[31,32].

Recent high-pressure studies of AFe$_2$O$_4$ (A= Zn, Mg, Co and Fe) ferrite spinels revealed a structural transition in between 25–30 GPa to a post-spinel phase[22,23,26,33–39] characterized by the *Cmcm* structure containing 6 and 8-fold coordination Fe^{3+} polyhedra[26]. With this, we note that lithium ferrite LiFe$_5$O$_8$ is the only member of the spinel ferrite family, which can be prepared in ordered and disordered phases[40], α-LiFe$_5$O$_8$ and β-LiFe$_5$O$_8$, respectively[41,42]. This feature makes LiFe$_5$O$_8$ especially attractive in terms of studying not only the pressure-induced site-selective Mott transition but also the influence of a structural disorder on this phenomenon.

In the present work, we reveal a pure site-selective Mott IMT in α-LiFe$_5$O$_8$ not complicated by any structural and spin transformation, and resulting in the formation of a site-selective Mott phase consisting of metallic/nonmagnetic and insulating sublattices. Furthermore, we find that electron delocalization in LiFe$_5$O$_8$ octahedral sublattice is a sluggish process due to a significant inhomogeneity of the iron local environment. Our results suggest that site-selective Mott transitions involving the formation of sublattices, which differ in their physical properties, within the same material, may constitute a rather general phenomenon in correlated-electron materials with a complex crystal structure.

Results

X-ray diffraction

XRD patterns obtained up to about 83 GPa are shown in Fig. 1a, and Supplementary Fig. 1 and 2. Low pressure (LP) patterns up to 36 GPa can be identified as the cubic phase with space group $P4_332$ with Fe^{3+} in tetrahedral (8*c*) and octahedral (12*d*) sites, whereas Li$^+$ ions occupy the (4*b*) octahedral positions (Supplementary Fig. 3a)[40]. At 33.6 GPa, new diffraction peaks start appearing. However, the LP cubic phase still dominates up to about 50 GPa and coexists with a new high-pressure (HP) phase nearly up to 57 GPa, after which no signature of the LP phase is found. Rietveld refinement was used in order to obtain lattice parameters for the LP phase according to space group $P4_332$ as seen in Supplementary Fig. 4i. The LP phase $V(P)$ data can be fit well with a second-order Birch-Murnaghan (BM2) equation of state (EOS)[43] (Fig. 1c, and Supplementary Table 1). (Supplementary Materials). The patterns of the HP phase could be fitted (Supplementary Fig. 4(ii)) well with the CaTi$_2$O$_4$-type (*Cmcm*) structure. This structure is characterized by two cationic sites: octahedral 8*f* and a bicapped trigonal prism 4*c* Wyckoff sites, characterized by 6 and 8-fold coordination polyhedra, respectively (Supplementary Fig. 3b). The structural transition to the HP phase is accompanied by ~ 2.1% volume reduction. Another noticeable change in the $V(P)$ data, namely a steeper decrease of the unit-cell volume of the HP phase with pressure increase occurs at about 70 GPa (Fig. 1(c)). Such $V(P)$ behavior

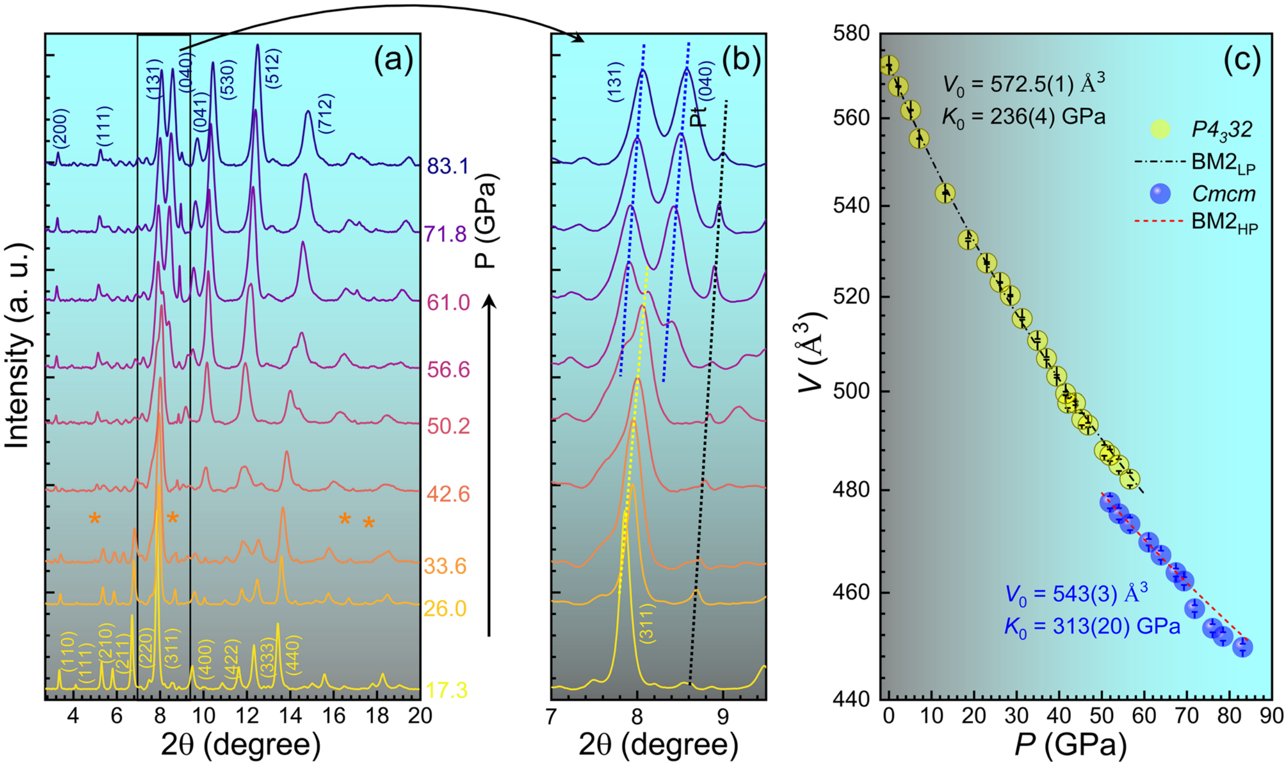

Fig. 1 | High-pressure Synchrotron x-ray diffraction results of α-LiFe$_5$O$_8$. a X-ray powder diffraction patterns of α-LiFe$_5$O$_8$ at T=298 K at various pressures (λ = 0.3344 Å). Diffraction peaks of the *Cmcm* high-pressure phase, which first appears at ~ 34 GPa (marked with asterisks) is clearly seen at 61 GPa. Miller indices in blue color correspond to the diffraction peaks of the *Cmcm* phase, whereas those in yellow represent peaks of the $P4_332$ phase. **b** Zoomed portion of the plot clearly showing structural phase transition. Positions of main diffraction peaks of the Pt pressure marker are shown with dashed lines. **c** Unit-cell volume of the various structural phases of α-LiFe$_5$O$_8$ as a function of pressure. Dash-dotted line is a fit for the cubic $P4_332$ phase using the BM2 EOS. The dotted line represents a fit to the orthorhombic *Cmcm* phase at the pressure range 51–69 GPa. Note a steeper decrease of unit-cell volume with pressure increase above 69 GPa. The volume and pressure error bars are within the symbol sizes.

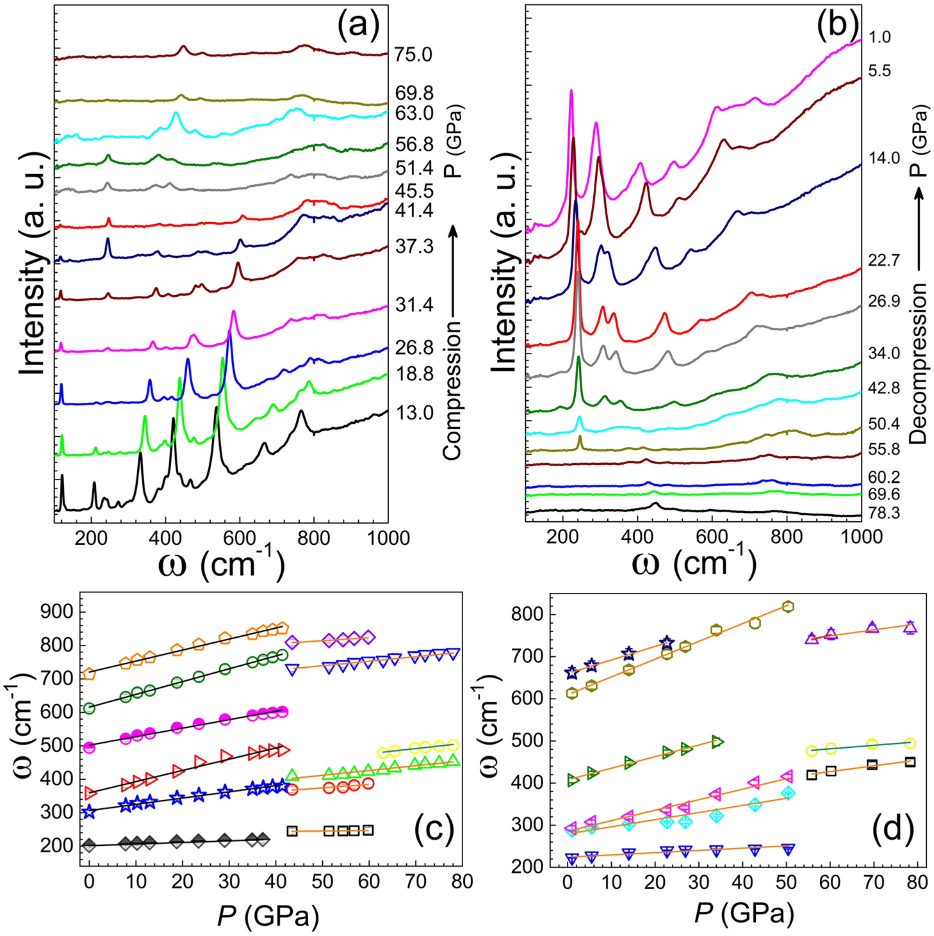

Fig. 2 | Raman spectra as a function of pressure. Raman spectra of α-LiFe$_5$O$_8$ at various pressures upon (**a**) compression up to ~ 78 GPa and (**b**) decompression. **c** Variation of the peak positions of the most intense Raman modes as a function of pressure for compression and (**d**) decompression cycles.

suggests an appreciable electronic transformation taking place within the HP phase. Correspondingly the $V(P)$ data for the HP phase could not be fitted with a "standard" equation of state. Meanwhile, one can use the data at a pressure range of $51<P<69$ GPa to define an EOS for the HP phase before the steeper decrease of V (Supplementary Table 1). An extrapolation of the obtained EOS to higher pressures allows us to estimate a volume reduction corresponding with the proposed electronic transition (Fig. 1c). This estimation gives $\Delta V/V_{70GPa} \approx 0.9\%$.

Raman spectroscopy

Room temperature Raman spectra of α-LiFe$_5$O$_8$ were collected up to nearly 78 GPa. The spectra measured upon compression are shown in Fig. 2a. Up to ~41 GPa all the peaks can be identified as the Raman modes calculated for α-LiFe$_5$O$_8$ sample in the $P4_332$ space group[44]. The appearance of new Raman peaks and the disappearance of previous ones can be seen above 41 GPa (Fig. 2a), suggesting a first-order structural transition at this pressure range. Another distinct change in the spectra can be seen above 60 GPa, above which some of the modes significantly decrease in intensity and an additional mode appears around 480 cm^{-1}. The results of the Raman measurements are summarized in Fig. 2c by plotting the most intense peak positions as a function of wavenumber. Two distinct changes can be seen at ~41 and 61 GPa as discussed above. Upon decompression, a distinct change in the Raman modes is observed at ~55GPa (Figs. 2b, d) with the recovery of the peaks, which remain down to ambient pressure. These peaks do not match with the LP structure but are consistent with the modes observed at the range 41–61 GPa upon compression. This suggests an irreversible structural phase transition in LiFe$_5$O$_8$, similar to other spinel ferrites[26].

Mössbauer spectroscopy

α-LiFe$_5$O$_8$ is ferrimagnetic below ~ 900 K[40]. At ambient conditions, the Mössbauer spectrum of LiFe$_5$O$_8$ consists of two sextets (Fig. 3a) corresponding to two LP Fe^{3+} structural sites, tetrahedral (T) and octahedral (O) (Supplementary Fig. 3a). The two components exhibit magnetic hyperfine fields H_{hf} = 49.7(2) and 51.6(2) T, typical for a ferric-oxide high-spin $^6A_{1g}$ state in tetrahedral and octahedral environments, respectively. The area ratio for these two components is restricted to 40:60 to remain consistent with the structural data discussed earlier. Between ambient pressure and 44 GPa the observed spectra barely change, with the only observable variation being a slight decrease in isomer shift and H_{hf} (Fig. 3d).

Above 52 GPa two new sextets appear (Figs. 3a, d) with smaller hyperfine field values of 41.6(9) and 35.7(1.7) T, suggesting Fe^{3+} HS states characterized by a magnetic ordering temperature (T_N) close to room temperature. These two new components, designated as HP1 and HP2, are characterized by isomer shift values of 0.23(4) and 0.36(3) mm/s (Fig. 3d). The larger isomer shift value obtained for the HP2 component suggests an 8-fold coordinated nearest-neighbor environment characterized by larger Fe–O distances (isomer shift has a negative linear dependence on the effective s-electron density at the nucleus $\rho_s(0)$[45]). Furthermore, the isomer shift values for the HP1 and LP(O) components are reasonably close supporting similar nearest-neighbor environments; namely, an octahedral configuration. Magnetic sextets from the LP phase coexist with the two new sextets up to at least 59 GPa (Figs. 3a, d). At 65 GPa, no traces of the LP phase have been found in the Mössbauer spectra. Alongside the magnetic sextets a non-magnetic component, designated as HP3, is observed in the central part of the spectra, characterized by a reduced isomer shift value of 0.19(2) mm/s. The abundance of the new component increases with pressure, replacing the

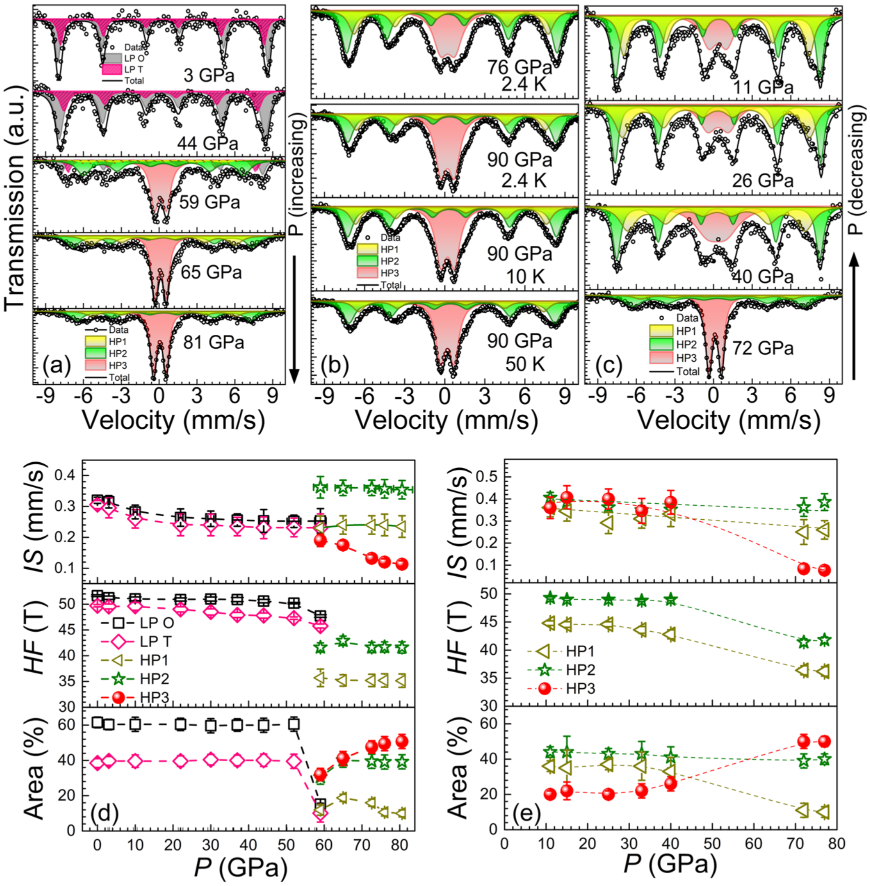

Fig. 3 | High-pressure Mössbauer spectroscopy results at ambient and low temperature. Selected Fe Mössbauer spectra of α-LiFe$_5$O$_8$ at various pressures and temperatures; at room temperature **a**, **c** and low temperatures **b**, upon compression **a**, **b** and decompression (**c**). Empty circles represent experimental data points whereas the black solid line through the data points represents the overall fit to the data from the sum of sub-components shown. Gray and pink shaded sub-components refer to the $P4_332$ phase tetrahedral and octahedral sites, respectively, whereas olive dark-yellow and red sub-components represent the *Cmcm* phase HP1, HP2, and HP3 components, respectively. Pressure dependence of the isomer shift (IS), hyperfine field (HF) and abundances or area percentage extracted from best fits to the Mössbauer spectra of α-LiFe$_5$O$_8$ for (**d**) compression and (**e**) decompression cycles at RT. In (**d**) black squares and pink diamonds refer to parameters for the octahedral and tetrahedral sites of the $P4_332$ phase, respectively, whereas dark yellow triangles, olive asterisks and red spheres in both (**d**) and (**e**) represent HP1, HP2 and HP3 components for the *Cmcm* phase, respectively. We note that in the case of SMS measurements (panel **b**) there is an appreciable delay in the HP1 to HP3 transformation compared to in-house measurements (panel **a**): even at 90 GPa the abundance of the HP1 component remains rather high, ~ 20%. This may be attributed to the different pressure transmitting media used and how the degree of non-hydrostaticity (strain and stress) affects the electronic transition[58].

HP1 component (Figs. 3a, d) and its isomer shift value shows an appreciable decrease above 65 GPa. Meanwhile, the abundance of the HP2 HS component stabilizes above 60 GPa at ~ 40% and does not change with pressure.

The HP3 component, observed above 65 GPa, can originate from a non-magnetic state or a low-spin state. To clarify the nature of this component we performed low–temperature Synchrotron MS measurements[46] at temperatures down to 2.4 K(Fig. 3b). (We note that when fitting the area ratio for the $P4_332$ phase we obtain the expected 60:40 in agreement with the structural data, but when all parameters are free, the uncertainty is large due to the overlap of the two components. Thus, we fixed the ratio at 60:40 to avoid larger uncertainty.). These measurements show no sign of broadening or splitting of the absorption spectrum and no increase of quadrupole splitting for HP3 component with temperature decrease down to 2.4 K, which means no features of a magnetic interaction. The collapse of magnetic interactions, observed above ~ 65 GPa, coinciding with the sharp decrease of the isomer shift (which means an increase of the effective s-electron density at the nucleus $\rho_s(0)$[45]) point to a collapse of electron localization rather than a transition to a low-spin state (see[9,10,45]).

Upon decompression, we do not observe a recovery of the original spectra typical for the LP phase. However, below 50 GPa the features of the spectra change significantly, compared to the spectra observed above 70 GPa (Figs. 3c, e). Particularly, the feature of the non-magnetic doublet changes with pressure decrease: it broadens considerably, decreases in magnitude and the corresponding isomer shift value increases by ~ 0.2 mm/s, almost coinciding with the isomer shift value of the HP1 component. In addition, H_{hf} values of the magnetic HP2 and HP1 components increase to about 49 and 43 T, respectively, suggesting an increase of the T_N values. One can propose a partial collapse of the magnetic order of the HP1 component, showing a central peak representing the fast spin-spin relaxation typical of the $T \sim T_N$ regime. The observed features of MS spectra upon decompression are undoubtedly a signature of an irreversible phase transition.

Electrical resistance

Room-temperature resistance for both compression and decompression cycles are shown in Fig. 4 as a function of pressure. A steep decrease in the resistance is observed at the 65–70 GPa pressure range, concurring with the growing of the non-magnetic doublet in Mössbauer spectra. The variation of ln$R$ as a function of inverse temperature at various pressures are shown in the inset of Fig. 4. Up to 63 GPa, the resistance increases with decreasing temperature, indicating insulating-like behavior. Above 65 GPa, the resistance shows metallic behavior. The activation energy E_a(P) obtained from the slope of linear fits to these plots is shown in the upper inset of Fig. 4: a continuous decrease in the E_a with increasing pressure results in a gap closure at ~ 68 GPa.

Upon decompression, down to 60 GPa the $R(P)$ behavior is similar to that of the compression cycle, indicating a pure electronic nature of the transition observed at the 60–70 GPa range. Upon further pressure decrease the $R(P)$ behavior changes significantly. The resistance value at ambient pressure is above two orders of magnitude lower compared to the compression cycle, despite the decrease in sample thickness. This agrees well with the signs of an irreversible structural phase transition, in accordance with Raman and MS data.

Discussions

Summarizing the obtained XRD, Raman spectroscopy and MS data, we can conclude that LiFe$_5$O$_8$, similar to a few other ferric spinels MFe$_2$O$_4$ (M=Fe, Mg, Zn)[22,23,26,33–38], undergoes a first order structural phase transition upon pressure increase; however, at the pressure range 33–57 GPa compared to 25–40 GPa typical for other ferric spinels. This phase transition is

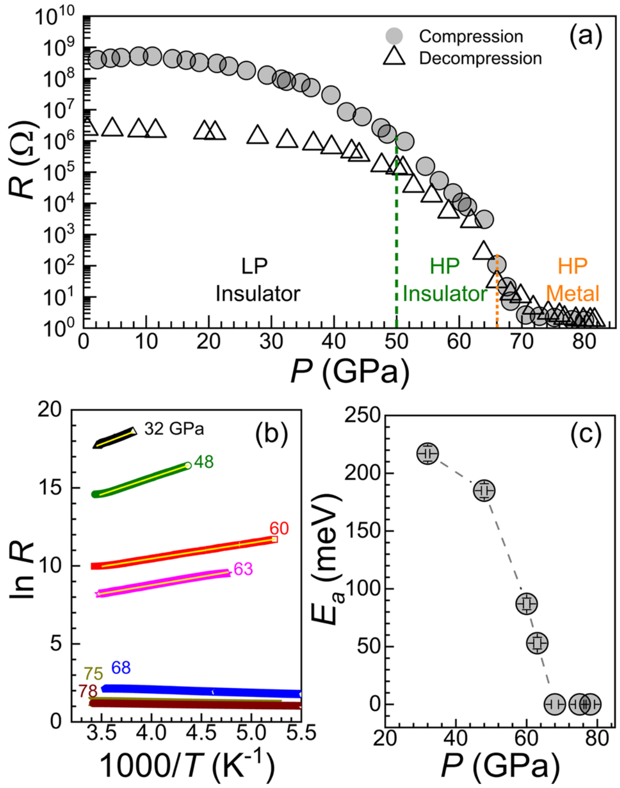

Fig. 4 | Electrical transport properties of α-LiFe$_5$O$_8$ as a function of pressure and temperature. **a** Pressure dependence of the resistance upon compression and decompression at 300 K in the main panel. Dashed green vertical line in the panel (**a**) delineates pressures where the new *Cmcm* phase starts to dominate according to XRD experiments (see text and preceding Fig. 1). Dashed orange line delineates the pressure where the insulator-to-metal transition takes place. The error in the pressure determination also should be taken into account. **b** shows linearized temperature-dependent data at various pressures assuming Arrhenius activated hopping transport (below 32 GPa such measurements were unrealizable using our experimental setup because of the high resistance value). The activation energy E_a is obtained from the slope of linear fits to these plots to obtain the charge gap for intrinsic conduction $E_g = 2E_a$. (**c**) shows the pressure dependence of E_a, which drops to zero at ~ 65 GPa.

manifested by the observed changes in XRD patterns, Raman spectra and dramatic changes of the hyperfine interaction parameters. As in many other ferrites, the high-pressure phase of LiFe$_5$O$_8$ comprises two distinct Fe^{3+} sites characterized by different H_{hf} and IS values. Analysis of the powder XRD data allows assuming for the HP phase the *Cmcm* structure typical for ferric[26] and some ferrous post-spinels[28–30]. In this structure, two Fe^{3+} sites, distinct according to MS studies, correspond well with two cationic sites: namely, the octahedral and a bicapped trigonal prism, characterized by 6 and 8-fold coordination polyhedra, respectively. The abundances of Fe^{3+} occupying octahedrons and bicapped trigonal prisms stand at 60:40% (Fig. 3c), respectively, which suggests that the rest of the octahedral sites are occupied by Li^{+1} ions.

Similar to the above-mentioned ferric spinels, immediately following the phase transition Fe^{3+} in both sites is in the HS state. With further pressure increase, a steeper decrease of unit-cell volume of the HP phase is seen at ~ 70 GPa (Fig. 1d). This behavior of the unit-cell volume corroborates with an appreciable change in the features of the MS spectra: namely, a new non-magnetic quadrupole-split component appears above ~ 59 GPa, with abundance increasing rapidly with pressure (Fig. 3c). The new HP3 component is characterized above 65 GPa by a significantly reduced IS value, which corresponds to an increase of the effective *s*-electron density at the nucleus that may result from either (*i*) a spin crossover, or (*ii*) a correlation breakdown (a Mott transition) in which magnetic interactions vanish[10,45]. In the present case, the lack of any signs of magnetic correlations on Mössbauer timescales (≈ 10^{-7} s) down to 2.4 K prompted us to designate the HP3 component as a non-magnetic resulting from an electron correlation breakdown. A corroborating IMT deduced from $R(P, T)$ measurements, confirms this conclusion. Since MS observations refer to the HP1 component as undergoing an electronic transition, we conclude that the Mott transition originates only on the octahedral sites, while the electronic state of Fe^{3+} ions on the trigonal prisms does not change at least up to ~ 90 GPa.

The existence of a site-selective Mott phase has recently been discussed in the rare-earth nickelates[15,16,47]. However, the latter remains electrically insulating, while exhibiting formation of site-selective local moments. Furthermore, recent studies of Fe$_2$O$_3$ provide an evidence for a site-selective Mott phase, in which the *3d* electrons on only half of the Fe sites (octahedral) are metallic, while the rest remain insulating[17]. However, in Fe$_2$O$_3$ the electronic transition coincides with the structural transition complicating an analysis of the role of structural and electronic components in the phase transition. In contrast to Fe$_2$O$_3$, in the present case we observe a pure electronic site-selective Mott transition not complicated by any structural transformations, which takes place in the *Cmcm* phase above 65 GPa. This transition is accompanied only by a minor volume decrease of ~ 0.9% suggesting a decrease of the FeO$_6$ octahedral volume below 2%. Such octahedral volume change at the transition is significantly less than that observed in Fe$_2$O$_3$ (~ 14 %), which signifies a different mechanism of the electronic transition in both cases. In Fe$_2$O$_3$ the octahedral volume change upon metallization is similar to that observed in CaFe$_2$O$_4$, FeOOH and FeBO$_3$[48–50] ($\Delta V/V_{oct}$ ~ 12–12.4%) during the Fe^{3+} HS-LS transition, suggesting in accord with theoretical calculations[17] a closure of the Mott-Hubbard gap associated with a spin crossover[12–14]. (We note that differences in the Mott transition onset pressure identified by the four techniques is ascribed to the different pressure transmitting media and degrees of hydrostaticity in the DAC (see supplementary materials). Undoubtedly, such a mechanism is not relevant to the present case. In the present case it seems that a more suitable scenario is the transformation of electron states from localized to itinerant without an accompanying change of the spin state. In such a case, the corresponding volume change could be relatively small[10]. Therefore, one can expect in LiFe$_5$O$_8$ a closure of the gap on the octahedral sites driven by a classical bandwidth broadening mechanism[1,2] and resulting in the formation of a site-selective Mott phase consisting of metallic and insulating sublattices.

The question remains, why the behavior of LiFe$_5$O$_8$ is different from many other ferric oxides, characterized by the HS-LS transition of the Fe^{3+} in the octahedral environment at the 40–60 GPa pressure range[10,13,24–26]. This feature could be related to a significant octahedral distortion due to the presence of Li^{+1}, whose ionic radius exceeds that of Fe^{3+} by ~ 18%[51]. It could be proposed that an additional ~ 16% decrease of Fe ionic radii due to the transition to the LS state and a corresponding further increase of the octahedral distortion does not facilitate this electronic transition. Meanwhile, in the case of another lithium ferrite, LiFeO$_2$, a very sluggish second-order Fe^{3+} HS-LS transition is observed, starting at ~ 50 GPa and not completed even at ~ 100 GPa (however, in contrast to LiFe$_5$O$_8$, LiFeO$_2$ remains insulating at least up to 115 GPa).

An important feature distinguishing these lithium ferrites is that rocksalt LiFeO$_2$ and the *Cmcm* phase of LiFe$_5$O$_8$ are microscopic disorder systems due to the presence of Li^{+1} ions in the octahedral sublattice. It is noteworthy that according to Mott's argument[1,2], in the case of doping a transition to a metal takes place at some critical concentration n_c. However, in fact, the doping process not only introduces excess electrons but at the same time creates disorder since the dopant atoms are randomly distributed in the host lattice. As a result, the observed transition is continuous and cannot be understood purely in terms of a Mott transition. Thus an Anderson-Mott transition picture seems more adequate[31]. In our case a transition to a metal can be achieved by inducing a *d* band broadening at some critical pressure P_c. However, the pure Mott transition picture is inadequate also in this case since one has to deal simultaneously with

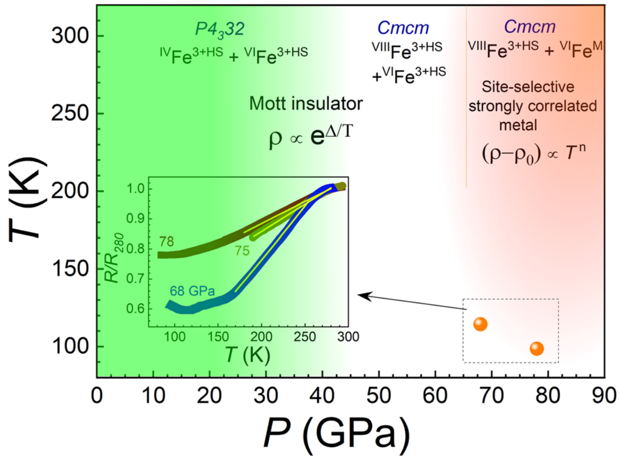

Fig. 5 | Pressure-temperature phase diagram of α-$LiFe_5O_8$. A part of the *R(T)* plot is expanded in the inset to emphasize the metallic behavior above ~ 65 GPa and the change of *R(T)* slope sign with temperature decrease. We note that a minimum in *R(T)* plots shifts to lower temperatures under pressure and above the minimum resistance shows $(R\text{-}R_0) \sim T^n$ behavior. Solid lines are fits using this expression where *n* value decreases gradually from $n \sim 1.19$ to 0.93 at the 68–78 GPa pressure range demonstrating a non-Fermi-liquid behavior.

disorder and interactions between the electrons. Correspondingly one would expect the transition, in part, to follow the Anderson model[52–54], and a continuous feature of the transition. Namely, a random distribution of Fe^{3+} and Li^{1+} cations in octahedral sites should result in significant inhomogeneity of the iron local environment, a possible clusters formation and therefore smearing the value of the critical pressure required for electron delocalization (or spin crossover in the case of $LiFeO_2$). Indeed, in contrast to many other ferric compounds[10] the Mott transition in $LiFe_5O_8$ is characterized by a rather gradual transformation. The onset of metallization is observed at ~ 65 GPa. However, according to SMS data (Fig. 3b), He pressure medium) about a third of octahedral Fe^{3+} ions (HP1 component) are still not involved in the transition and their fraction remains quite large up to ~ 90 GPa, the highest pressure measured. In the case of N_2 pressure medium the transition is sharper (Fig. 3a) suggesting that a transition diffuseness strongly depends on the hydrostatic conditions shaping the sample microstructure. Hence, another noticeable feature of the Mott transition in $LiFe_5O_8$ is the interplay between electron-electron interactions and disorder, which results in the sluggish second-order-type metallization on the octahedral sites associated with a nonhomogeneous environment of Fe^{3+} ions. This special case of the site-selective Mott transition is of great interest and undoubtedly deserves further in-depth study.

In Fig. 5 we present the pressure-temperature phase diagram of $LiFe_5O_8$ based on our XRD, MS, resistivity and Raman spectroscopy results. We note that $LiFe_5O_8$ turns metallic at $P_c \sim 65$ GPa but with a minimum in *R*(T) plots above P_c, which shifts to lower temperatures under pressure. The change of the *R*(T) slope sign at lower temperature could be related with a weak electron localization originating from the presence of disorder potentials in the octahedral sublattice. According to MS data this disorder results also in a smearing of the transition pressure range and an incompleteness of the electron delocalization process up to the highest pressures measured. Upon decompression, according to the Raman and MS data, the *Cmcm* structure remains unchanged. However, we observe a reversal in electronic properties with no sign of hysteresis down to ~ 60 GPa confirming a pure electronic nature of the observed site-selective electronic transition, not complicated by any coinciding structural transformations.

Conclusions

We provide experimental evidence for a pressure-induced site-selective Mott IMT in $LiFe_5O_8$ characterized by site-selective delocalization of electrons above 65 GPa. Within the *Cmcm* crystal structure, characterized by two distinct coordination sites (VI and VIII), we observe 40% of ferric ions occupying bicapped trigonal prism sites and above 65 GPa ions on the octahedral sites having delocalized electrons. The transition is characterized by delocalization/metallization of the *3d* electrons only on the Fe sites in the octahedral sublattice, with a site-dependent collapse of magnetic interactions. The delocalization of electrons on the octahedral sites coincides with a minor volume decrease suggesting a classical Mott IMT driven by a bandwidth broadening mechanism. Due to a significant inhomogeneity of the iron local environment in the octahedral sublattice, containing also Li ions, the electron delocalization is a sluggish process, which is not completed yet at about 90 GPa: instead of a certain critical pressure of the IMT one observes a broad critical pressures distribution. Hence, in the case of $LiFe_5O_8$ at high pressures the material is characterized by two sublattices, which differ significantly not only by the P_c value but also by the character of the IM transition. Thus, our results extend the classification of Mott insulator-to-metal transition, offering the documentation of a pure site-selective mechanism, not complicated by any structural and spin transformation, in this case–a second-order type. They suggest that the concept of a site-selective Mott transition may be applicable to correlated-electron materials: in particular, in materials with a complex crystal structure and intricate short-range ordering features.

Methods

A polycrystalline sample of α-$LiFe_5O_8$ was synthesized at Tel Aviv University (TAU) (enriched to 25% with ^{57}Fe isotope when needed for MS experiments). Custom TAU diamond anvil cells (DACs)[55] were used to induce high pressure, with He, Ne or N_2 as a pressure-transmitting medium. The pressure was determined using the ruby R1 fluorescence line as a pressure marker[56], diamond Raman spectra[57], and the Ne and Pt unit-cell volumes in the case of x-ray diffraction studies. Powder XRD experiments were performed at the 13-ID-D beamline of the Advanced Photon Source (APS), Argonne National Laboratory (Argonne, IL) and at the beamline of the Synchrotron Soleil (Paris). Diffraction patterns up to ~ 30 GPa were analyzed by Rietveld refinement and above ~ 30 GPa by using the Whole Profile Fitting (Pawley) method (see Supplementary Materials www.xxxxx.com). ^{57}Fe Mössbauer studies were performed using a 10 mCi ^{57}Co (Rh) point source. Low-temperature measurements at 76 and 90 GPa were performed using energy-domain synchrotron Mössbauer spectroscopy carried out at the beamline ID18 at ESRF (Grenoble). Electrical resistance measurements were performed as a function of pressure and temperature using a standard four-probe method. High-pressure Raman spectra of $LiFe_5O_8$ were collected at room temperature using a Horiba (iHr-550) spectrometer with a 487.8 nm excitation source. Further technical details about the methods used can be found in the Supporting Information www.xxxxx.com.

Data availability

The data sets supporting the findings of the present study are available from the corresponding author upon reasonable request.

Received: 3 May 2024; Accepted: 28 June 2024;

References

1. Mott, N. *Metal-insulator transitions* (CRC Press, 2004).
2. Mott, N. F. Metal-insulator transition. *Rev. Mod. Phys.* **40**, 677 (1968).
3. Imada, M., Fujimori, A. & Tokura, Y. Metal-insulator transitions. *Rev. Mod. Phys.* **70**, 1039 (1998).
4. Si, Q. & Abrahams, E. Strong correlations and magnetic frustration in the high T_c iron pnictides. *Phys. Rev. Lett.* **101**, 076401 (2008).
5. de'Medici, L., Giovannetti, G. & Capone, M. Selective mott physics as a key to iron superconductors. *Phys. Rev. Lett.* **112**, 177001 (2014).
6. Gebhard, F. *Metal—insulator transitions* (Springer, 1997).
7. Edwards, P. & Rao, C. N. R.*The Metal-Nonmetal Transition Revisited* (CRC Press, 2018).

8. Khomskii, D. I. et al. *Transition metal compounds* (Cambridge University Press, 2014).
9. Arielly, R. et al. Intriguing sequence of $GaFeO_3$ structures and electronic states to 70 GPa. *Phys. Rev. B* **84**, 094109 (2011).
10. Rozenberg, G. Kh., Xu, W. & Pasternak, M. P. The mott insulators at extreme conditions; structural consequences of pressure-induced electronic transitions. *Z. Kristallogr. Cryst. Mater.* **229**, 210–222 (2014).
11. Saxena, S. K. et al*. Advances In Physical Geochemistry*, vol. 2 (Springer Science & Business Media, 2012).
12. Kuneš, J., Lukoyanov, A. V., Anisimov, V. I., Scalettar, R. T. & Pickett, W. E. Collapse of magnetic moment drives the mott transition in MnO. *Nat. Mater.* **7**, 198–202 (2008).
13. Lyubutin, I., Ovchinnikov, S., Gavriliuk, A. & Struzhkin, V. Spin-crossover-induced mott transition and the other scenarios of metallization in 3d n metal compounds. *Phys. Rev. B* **79**, 085125 (2009).
14. Greenberg, E. et al. Mott transition in $CaFe_2O_4$ at around 50 GPa. *Phys. Rev. B* **88**, 214109 (2013).
15. Park, H., Millis, A. J. & Marianetti, C. A. Site-selective mott transition in rare-earth-element nickelates. *Phys. Rev. Lett.* **109**, 156402 (2012).
16. Subedi, A., Peil, O. E. & Georges, A. Low-energy description of the metal-insulator transition in the rare-earth nickelates. *Phys. Rev. B* **91**, 075128 (2015).
17. Greenberg, E. et al. Pressure-induced site-selective mott insulator-metal transition in Fe_2O_3. *Phys. Rev. X* **8**, 031059 (2018).
18. Layek, S. et al. Verwey-type charge ordering and site-selective mott transition in Fe_4O_5 under pressure. *J. Am. Chem. Soc.* **144**, 10259 (2022).
19. Goldman, A. *Modern Ferrite Technology* (Springer Science & Business Media, 2006).
20. Brabers, V. Progress in spinel ferrite research. *Handbook of Magnetic Materials* **8**, 189–324 (1995).
21. Van Groenou, A. B., Bongers, P. & Stuyts, A. Magnetism, microstructure and crystal chemistry of spinel ferrites. *Materials Science and Engineering* **3**, 317–392 (1969).
22. Levy, D., Pavese, A. & Hanfland, M. Phase transition of synthetic zinc ferrite spinel ($ZnFe_2O_4$) at high pressure, from synchrotron x-ray powder diffraction. *Phys. Chem. Miner.* **27**, 638–644 (2000).
23. Andrault, D. & Bolfan-Casanova, N. High-pressure phase transformations in the $MgFe_2O_4$ and Fe_2O_3–$MgSiO_3$ systems. *Phys. Chem. Miner.* **28**, 211–217 (2001).
24. Friedrich, A. et al. Pressure-induced spin collapse of octahedrally coordinated Fe^{3+} in $Ca_3Fe_2[SiO_4]$ from experiment and theory. *Phys. Rev. B* **90**, 094105 (2014).
25. Lyubutin, I. S. & Gavriliuk, A. G. Research on phase transformations in 3d-metal oxides at high and ultrahigh pressure: State of the art. *Phys.-Uspekhi* **52**, 989 (2009).
26. Greenberg, E. et al. High-pressure magnetic, electronic, and structural properties of MFe_2O_4 (M= Mg, Zn, Fe) ferric spinels. *Phys. Rev. B* **95**, 195150 (2017).
27. Layek, S. et al. Pressure-induced spin crossover in disordered *α*-$LiFeO_2$. *Phys. Rev. B* **94**, 125129 (2016).
28. Xu, W. et al. $FeCr_2O_4$ spinel to near megabar pressures: Orbital moment collapse and site-inversion facilitated spin crossover. *Phys. Rev. B* **95**, 045110 (2017).
29. Xu, W. et al. Site-specific spin crossover in Fe_2TiO_4 post-spinel under high pressure up to nearly a megabar. *Phys. Rev. B* **96**, 045108 (2017).
30. Xu, W. et al. Interplay between structural and magnetic-electronic responses of $FeAl_2O_4$ to a megabar: Site inversion and spin crossover. *Phys. Rev. B* **97**, 085120 (2018).
31. Belitz, D. & Kirkpatrick, T. The Anderson-Mott transition. *Rev. Mod. Phys.* **66**, 261 (1994).
32. Li, T. et al. Continuous mott transition in semiconductor moiré superlattices. *Nature* **597**, 350–354 (2021).
33. Finger, L. W., Hazen, R. M. & Hofmeister, A. M. High-pressure crystal chemistry of spinel ($MgAl_2O_4$) and magnetite (Fe_3O_4): comparisons with silicate spinels. *Phys. Chem. Miner.* **13**, 215–220 (1986).
34. Fei, Y., Frost, D. J., Mao, H.-K., Prewitt, C. T. & Haeusermann, D. In situ structure determination of the high-pressure phase of Fe_3O_4. *Am. Mineral.* **84**, 203–206 (1999).
35. Haavik, C., Stølen, S., Fjellvag, H., Hanfland, M. & Hausermann, D. Equation of state of magnetite and its high-pressure modification: thermodynamics of the Fe-O system at high pressure. *Am. Mineral.* **85**, 514–523 (2000).
36. Dubrovinsky, L. et al. The structure of the metallic high-pressure Fe_3O_4 polymorph: experimental and theoretical study. *J. Phys. Condens. Matter* **15**, 7697 (2003).
37. Greenberg, E. et al. On the compressibility of ferrite spinels: a high-pressure x-ray diffraction study of MFe_2O_4 (M= Mg, Co, Zn). *High Pressure Research* **29**, 764–779 (2009).
38. Xu, W., Machavariani, G. Y., Rozenberg, G. Kh. & Pasternak, M. Mössbauer and resistivity studies of the magnetic and electronic properties of the high-pressure phase of Fe_3O_4. *Phys. Rev. B* **70**, 174106 (2004).
39. Yamanaka, T., Uchida, A. & Nakamoto, Y. Structural transition of post-spinel phases $CaMn_2O_4$, $CaFe_2O_4$, and $CaTi_2O_4$ under high pressures up to 80 GPa. *Am. Mineral.* **93**, 1874–1881 (2008).
40. Verma, S. & Joy, P. Magnetic properties of superparamagnetic lithium ferrite nanoparticles. *J. Appl. Phys.* **98**, 124312 (2005).
41. Braun, P. A superstructure in spinels. *Nature* **170**, 1123–1123 (1952).
42. Tomas, A., Laruelle, P., Dormann, J. & Nogues, M. Affinement de la structure des formes ordonnée et désordonnée de l'octaoxopentaferrate de lithium, $LiFe_5O_8$. *Acta Crystallogr. C* **39**, 1615–1617 (1983).
43. Anderson, O. L. et al. *Equations of state of solids for geophysics and ceramic science*. 31 (Oxford University Press on Demand, 1995).
44. Iliev, M. et al. Lattice dynamics of the *α* and *β* phases of $LiFe_5O_8$. *Phys. Rev. B* **83**, 174111 (2011).
45. Gütlich, P., Bill, E. & Trautwein, A. X. *Mössbauer spectroscopy and transition metal chemistry: fundamentals and applications* (Springer Berlin, Heidelberg, 2010).
46. Potapkin, V. et al. The ^{57}Fe synchrotron Mössbauer source at the ESRF. *J. Synchrotron Radiat.* **19**, 559–569 (2012).
47. Middey, S. et al. Disentangled cooperative orderings in artificial rare-earth nickelates. *Phys. Rev. Lett.* **120**, 156801 (2018).
48. Merlini, M. et al. Fe^{3+} spin transition in $CaFe_2O_4$ at high pressure. *Am. Mineral.* **95**, 200–203 (2010).
49. Xu, W. et al. Pressure-induced hydrogen bond symmetrization in iron oxyhydroxide. *Phys. Rev. Lett.* **111**, 175501 (2013).
50. Xu, W. et al. Pressure-induced high-spin/low-spin disproportionated state in the mott insulator $FeBO_3$. *Sci. Rep.* **12**, 9647 (2022).
51. Shannon, R. D. Revised effective ionic radii and systematic studies of interatomic distances in halides and chalcogenides. *Acta Crystallographica Section A* **32**, 751–767 (1976).
52. Anderson, P. W. Absence of diffusion in certain random lattices. *Phys. Rev.* **109**, 1492 (1958).
53. Lee, P. A. & Ramakrishnan, T. Disordered electronic systems. *Rev. Mod. Phys.* **57**, 287 (1985).
54. Brandes, T. & Kettemann, S. *Anderson Localization And Its Ramifications: Disorder, Phase Coherence, And Electron Correlations* (Springer Berlin, Heidelberg, 2010).
55. Yu. Machavariani, G., Pasternak, M. P., Hearne, G. R. & Rozenberg, G. Kh. A multipurpose miniature piston-cylinder diamond-anvil cell for pressures beyond 100 GPa. *Rev. Sci. Instrum.* **69**, 1423–1425 (1998).
56. Dewaele, A., Torrent, M., Loubeyre, P. & Mezouar, M. Compression curves of transition metals in the mbar range: Experiments and projector augmented-wave calculations. *Phys. Rev. B* **78**, 104102 (2008).

57. Akahama, Y. & Kawamura, H. Pressure calibration of diamond anvil raman gauge to 310 GPa. *J. Appl. Phys.* **100**, 043516 (2006).
58. Glazyrin, K., Miyajima, N., Smith, J. S. & Lee, K. K. Compression of a multiphase mantle assemblage: effects of undesirable stress and stress annealing on the iron spin state crossover in ferropericlase. *J. Geophys. Res. Solid Earth* **121**, 3377–3392 (2016).

Acknowledgements

This research was supported by the Israeli Science Foundation (Grants No. 1189/14, No. 1552/18 and No. 1748/20). S. L. sincerely acknowledges Planning and Budget Commission from Higher Education Ministry of Israel for providing PBC post-doctoral fellowship. We thank Prof. J. Lashley for his interest in this research and for fruitful discussions. Authors are thankful to Mark Shulman for his help in the initial stages of a few experiments. We are grateful to J. P. Itié and the beamline team at the Synchrotron Soleil for their assistance in using beamline PSICHÉ. A few Mössbauer spectrum at low temperature were collected at the ID-18 beamline of the European Synchrotron Radiation Facility, Grenoble, France. We are grateful to D. G. Merkel for his assistance in using beamline ID-18. Portions of this work were performed at GeoSoilEnviroCARS (The University of Chicago, Sector 13), Advanced Photon Source (APS), Argonne National Laboratory. GeoSoilEnviroCARS is supported by the National Science Foundation - Earth Sciences (EAR - 1634415). This research used resources of the Advanced Photon Source, a U.S. Department of Energy (DOE) Office of Science User Facility operated for the DOE Office of Science by Argonne National Laboratory under Contract No. DE-AC02-06CH11357. S. L. sincerely acknowledge SEED (Grant No.: UPES/R&D-SOE/20062022/02) and SEED-INFRA (Grants No.: UPES/R&D-SEED-INFRA/24082023/04 and UPES/R&D-SoAE/08042024/20) research funding from UPES, Dehradun, India. S.S.S. would like to acknowledge support (Grants No.: G117669) from Department of Science Innovation and Technology, UK.

Author contributions

S.L., E.G., D.L., V.P., and G.K.R. conducted the experiments; S.L., E.G., and D.L. performed the data analysis; G.K.R., S.L., and S.S.S. conceived and supervised the project and wrote the paper. All the authors contributed to the writing of the final manuscript.

Competing interests

The authors declare that they have no competing interests.

Additional information

Supplementary information The online version contains supplementary material available at https://doi.org/10.1038/s43246-024-00560-x.

Correspondence and requests for materials should be addressed to Samar Layek or Gregory Kh. Rozenberg.

Peer review information *Communications Materials* thanks the anonymous reviewers for their contribution to the peer review of this work. Primary Handling Editor: Aldo Isidori.